Advanced Composites and Hybrid Materials (2025) 8:423
https://doi.org/10.1007/s42114-025-01510-y

RESEARCH

Multifunctional Janus organic hydrogel enables in situ wound visual monitoring and healing

Yu Cheng[1] · Sen Li[2] · Siqi Liang[3] · Zhengkun Yi[4] · Yu Chang[5] · Yi Zhang[6] · Bin Sun[1] · Tao Peng[1] · Shaohui Wu[7] · Jing Li[3] · Hui Yang[1] · Hongyan Sun[1]

Received: 6 May 2025 / Revised: 17 September 2025 / Accepted: 17 October 2025
© The Author(s) 2025

Abstract

Rapid wound closure is crucial to prevent microbial invasion during skin trauma. Delayed diagnosis and treatment of wound infection may lead to complications such as impaired healing and sepsis. Conventional clinical dressings (e.g., cotton and gauze) mainly provide physical isolation but fail to establish an antibacterial microenvironment. These dressings often adhere to wound tissues, resulting in secondary injury during removal, and lack the capability for real-time monitoring of wound conditions. This study innovatively integrates multimodal pressure sensing with wound repair functions, enabling the synergistic development of smart sensing wound dressings (SSWD) that offer real-time visual monitoring. The dressing employs gradient cross-linking to fabricate a dynamic self-adaptive Janus-structured organic hydrogel. The upper non-adhesive ion-sensing layer incorporates micro-nano surface structures, enabling high-resolution real-time responses to mechanical signals from wound swelling and tissue regeneration. This capability, when coupled with an image acquisition system, enables visual monitoring of the healing process. The lower adhesive layer ensures robust interfacial integration with the wounds' bed via hydrogen bonding while allowing controlled sustained release of drugs that promote healing. This system propels the development of intelligent dressings towards diagnosis-treatment integration and offers an innovative solution for precision wound management.

Keywords Iontronic pressure sensing · Smart sensing wound dressings · Janus organic hydrogel · Wound healing · Wound status monitoring

Yu Cheng, Sen Li and Siqi Liang contributed equally to this work.

✉ Jing Li
lijing52@shnu.edu.cn

✉ Hui Yang
hui.yang@siat.ac.cn

✉ Hongyan Sun
hy.sun@siat.ac.cn

[1] Bionic Sensing and Intelligence Center (BSIC), Institute of Biomedical and Health Engineering, Shenzhen Institutes of Advanced Technology, Chinese Academy of Sciences, Shenzhen, Guangdong 518055, China

[2] School of Engineering, Hangzhou Normal University, Hangzhou, Zhejiang 311121, China

[3] College of Life Sciences, Shanghai Normal University, Shanghai 200234, China

[4] The Guangdong Provincial Key Laboratory of Robotics and Intelligent System, Shenzhen Institutes of Advanced Technology (SIAT), Chinese Academy of Sciences (CAS), Shenzhen, Guangdong 518055, China

[5] Center for Intelligent Medical Equipment and Devices (iMED), Suzhou Institute for Advanced Research, University of Science and Technology of China, Suzhou, Jiangsu 215123, China

[6] Institute of Biomedical and Health Engineering, Shenzhen Institutes of Advanced Technology, Chinese Academy of Sciences, Shenzhen, Guangdong 518055, China

[7] Department of Cardiology, Shanghai Chest Hospital, School of Medicine, Shanghai Jiao Tong University, 241 West Huaihai Road, Xuhui District, Shanghai 200030, China

Published online: 13 November 2025

1 Introduction

Skin is the first defense that protects the body's tissues and organs from external harm, playing an indispensable role in maintaining overall health and safety of the body. When the damaged skin is subjected to improper wound care, it will cause repeated infections or persistent inflammation, which greatly hinders the normal recovery process of the wound [1]. The wound healing process is a dynamic and continuous process comprised of four overlapping stages: hemostasis, inflammation, proliferation, and remodeling [2]. Traditional wound gauze has limitations in practical application, such as being prone to adhere to the wound and lacking self-antimicrobial capabilities. It requires frequent replacements to clean the wound and avoid wound adhesion, failing to provide real-time monitoring of the wound status, thus bringing obvious discomfort and pain to the patient and hindering wound recovery [3]. Therefore, the development and adoption of more advanced wound care methods are of great significance for promoting wound healing, alleviating patient suffering, and optimizing the allocation of medical resources [4].

Hydrogels have emerged as a promising alternative to achieve functional recovery of damaged skin tissue due to their high water content, tissue-like mechanical properties, and ability to provide a favorable moist environment for wound regeneration and epithelialization [5]. More importantly, hydrogels can be functionalized by introducing bioactive molecules or changing cross-linking networks to endow them with multifunctional properties such as hemostasis, antibacterial, and tissue adhesion, making them ideal wound dressings to promote wound healing [6, 7]. He et al. developed an injectable hydrogel adhesive through a catalyst-free o-phthalaldehyde/amine (hydrazide) cross-linking reaction. In the full-layer skin incision model of rats and rabbits, the hydrogel adhesives can quickly close the incision to accelerate the wound healing [8]. Pu et al. proposed a composite hydrogel that can self-regulate the release of cupric ions and luteolin, and modulate mechanical properties to promote chronic wound healing [9]. With recent research and development progress, the function of hydrogels has evolved from simple physical coverage or single function to a combination of multiple advanced functions towards greater intelligence, such as anti-inflammatory, antibacterial, and accelerating healing [10].

The rapid development of flexible electronics has brought revolutionary progress to intelligent healthcare, especially in the field of wound healing and wound status monitoring [11–13]. Research in this field focuses on the development of intelligent materials and devices that can actively promote the healing process [14, 15]. The physical and biochemical parameters at the wound site are important indicators of the wound healing process, including temperature, pH, uric acid, glucose, inflammatory mediators, and pressure, among others, serving as crucial inputs for wound management [16, 17]. For instance, Khademhosseini et al. proposed a smart and automated flexible wound dressing that integrates temperature and pH sensors onto flexible bandages, which can monitor the wound status in real-time and significantly affect the treatment of chronic wounds [18]. Zhang et al. proposed a novel strategy combining an intelligent hydrogel microneedle pH sensor to inhibit wound infection and track wound healing status, providing a convenient method for disease diagnosis and personalized health management [19]. Yu et al. proposed an electrostatic induction–enabled anti-touching hydrogel dressing that promotes wound healing and prevents secondary injury to wounds caused by accidental contact [20]. Although researches have been reported assessing wound status by monitoring parameters such as temperature, pH, and glucose levels, there are few studies that directly reflect wound recovery status by perceiving the shape, size, and surface hardness of the wound. The development of flexible pressure sensing technology offers a potential solution to this challenge [21]. This technology can reflect the recovery status of wounds by detecting physical parameters related to the wound, such as pressure and deformation. Pressure sensors can be classified into four different types based on their sensing mechanisms: piezoresistive [22, 23], capacitive [24, 25], piezoelectric [26, 27], and triboelectric [28, 29]. Among these, a new capacitive pressure sensing mode, known as iontronic sensing, utilizes the supercapacitive properties of the electrical double layer (EDL) at the electrolytic-electronic interface, resulting in ultrahigh sensitivity, high noise resistance, high resolution, and response to both static and dynamic stimuli [30]. Iontronic sensors rely on ionic-active materials to construct thin and flexible device architectures, meeting requirements of on-body wearable systems, especially in the health and medical field [31].

Asiaticoside has been widely used for skin injuries owing to its effective antibacterial, anti-inflammatory, and healing functions in traditional hydrogel dressings. By combining asiaticoside with smart hydrogels to construct functional wound dressings that integrate wound repair, antibacterial/anti-inflammatory properties, and pressure sensing capabilities, it enables the integration of the bioactive advantages of natural pharmaceuticals, material multifunctionality, and intelligent sensing technology. This innovation is expected to transcend the limitations of "passive repair" inherent in conventional dressings, ultimately realizing a "sensing-response-treatment" functional system. According to the above hypothesis, we have innovatively integrated pressure sensing with wound dressing to develop a smart sensing wound dressing (SSWD), which not only promotes wound

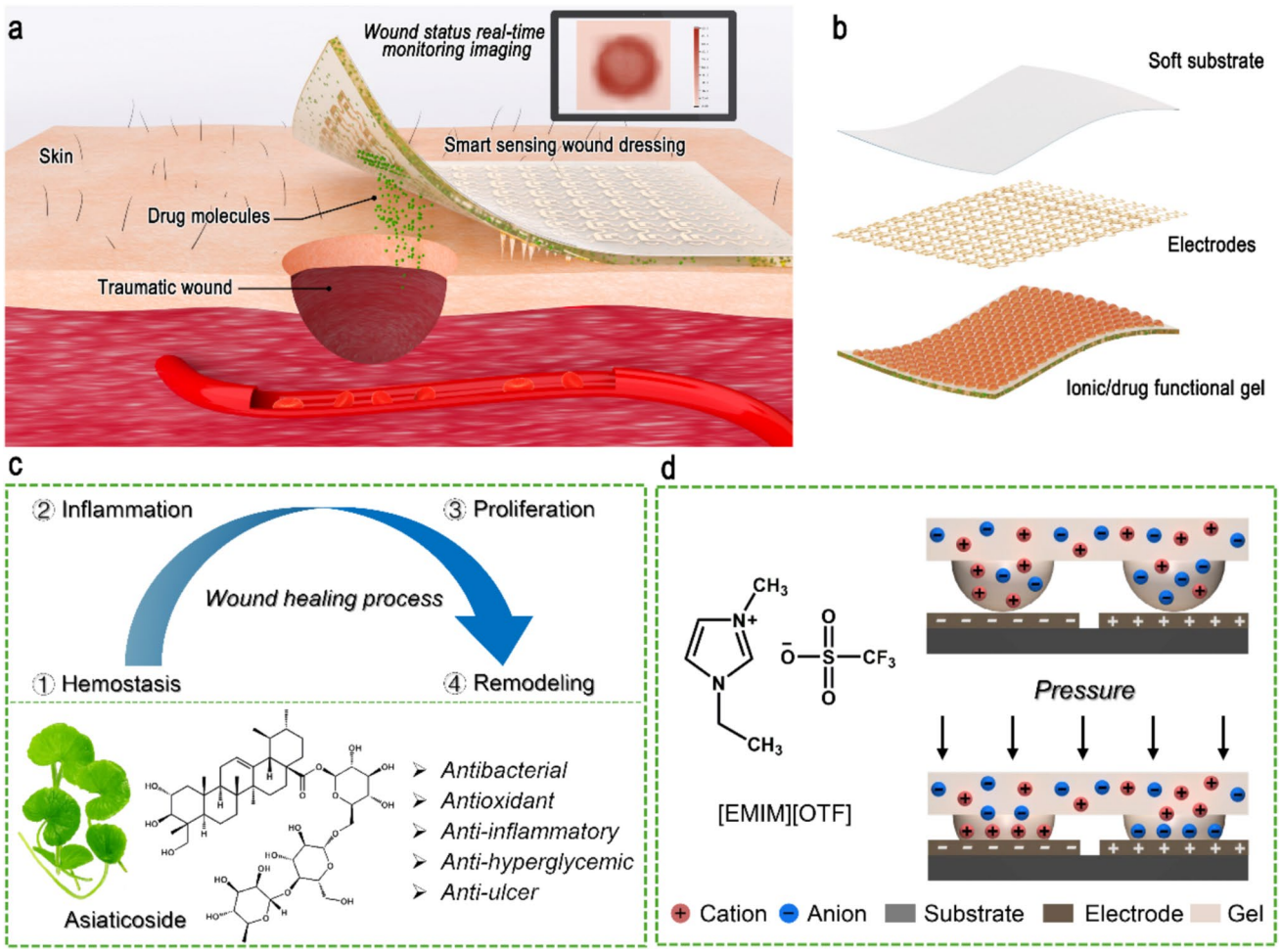


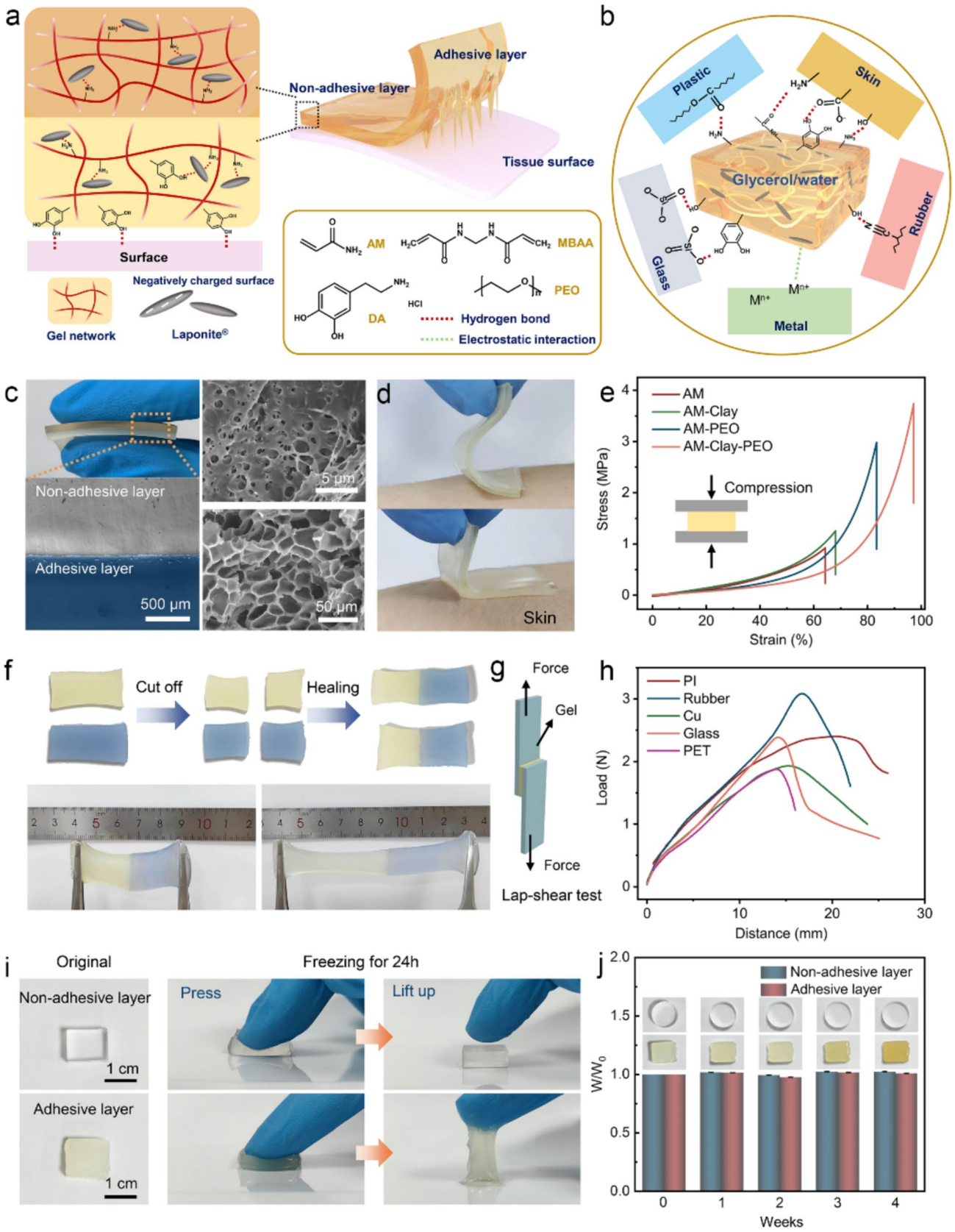
Fig. 1 Overall schematic and design strategies of smart sensing wound dressing. **a** Schematic image of a multifunctional wound dressing designed for healing traumatic wounds and visually monitoring the wound state. **b** Exploded view schematic illustrating the smart wound dressing composed of functional gel, electrodes, and soft substrate. **c** Four stages of wound healing and advantages of asiaticoside structure. **d** Mechanical response principle of the smart wound dressing for contact pressure detection

healing but also monitors wound swelling and growth status in real time, enabling visual monitoring through high-density sensor array imaging. We present a multifunctional Janus organic hydrogel with high flexibility, self-healing, biocompatibility, anti-freezing, and moisturizing properties. The upper layer of the Janus gel, containing ionic liquid with its non-adhesive properties, serves as an iontronic pressure sensor that responds to external stimuli and reverts to its original state upon stimulus removal, while its micro and nano surface structures facilitate pressure sensing and visual monitoring of wound conditions. The lower layer is viscous, able to firmly adhere to the wound surface, and can be infused with drug molecules to promote healing, forming an effective wound dressing. When connected to an image acquisition device, the SSWD enables digital remote real-time monitoring and diagnosis, providing healthcare professionals with more precise information on wound surface status to facilitate patient treatment.

2 Results and discussion

2.1 Design and structure of smart sensing wound dressing

The proposed SSWD, consisting of multifunctional Janus organic hydrogel and flexible electrode, offers comprehensive wound management, including healing promotion and visual pressure monitoring, as shown in Fig. 1a. The Janus organic hydrogel has been designed to perform different functions on both sides. The lower layer, adhering closely to the skin, contains one herbal extract, asiaticoside, which assists healing via continuously releasing drugs to the wound bed. The upper layer of the Janus organic hydrogel integrates with the flexible electrode covered on it to form a pressure sensing system and monitor the wound condition. Figure 1b illustrates the entire structure of the SSWD, which consists of (i) a functional gel with ionically


a
Adhesive layer
Non-adhesive layer
Tissue surface
Surface
Negatively charged surface
Gel network
Laponite®
AM
MBAA
PEO
DA
HCl
Hydrogen bond
Electrostatic interaction
b
Plastic
Skin
Glycerol/water
Glass
Rubber
Metal
c
Non-adhesive layer
Adhesive layer
500 μm
5 μm
50 μm
d
Skin
e
AM
AM-Clay
AM-PEO
AM-Clay-PEO
Compression
Stress (MPa)
Strain (%)
f
Cut off
Healing
g
Force
Gel
Force
Lap-shear test
h
PI
Rubber
Cu
Glass
PET
Load (N)
Distance (mm)
i
Original
Freezing for 24h
Non-adhesive layer
Adhesive layer
1 cm
Press
Lift up
j
Non-adhesive layer
Adhesive layer
W/W0
Weeks

◂**Fig. 2** Characterization of Janus organic hydrogel. **a** Structural schematic and chemical composition of the Janus organic hydrogel with the adhesive and non-adhesive layers. **b** Schematic depicting the adhesion mechanism between the adhesive gel and various substrates. **c** Morphology images of the two gel layers. **d** Adhesion difference between the two gel layers towards the skin. **e** Compressive curves of different gel components. **f** Self-healing property of the adhesive gel layer. **g** Schematic of the lap-shear test. **h** Adhesive force vs displacement curves for the adhesive gel adhered to various substrates. **i** Anti-freezing properties of both the adhesive and non-adhesive layers. **j** Long-term stabilities of both layers

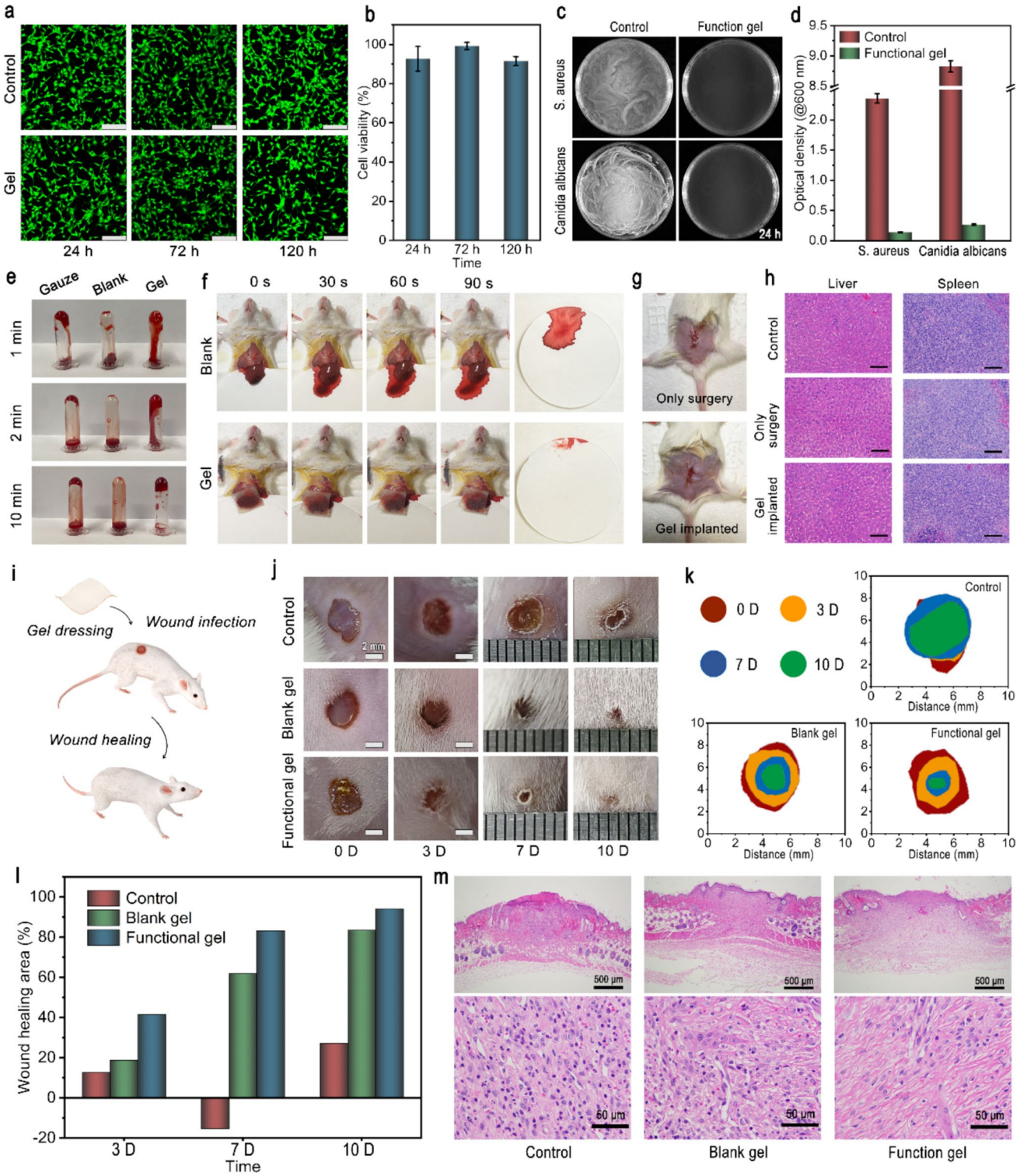
active elastic micro-structures and drug-loaded adhesion on both sides, respectively, and (ii) a stretchable electrode layer on a soft membrane serving as the upper substrate and packaging for structural integrity. The wound healing process involves four stages: hemostasis, inflammation, proliferation, and remodeling. Preferred wound dressings can not only be effective for different stages of healing, while also being able to cope with complex environments during the wound healing process (such as external infections). Extracted from the umbelliferae plant *Centella asiatica*, asiaticoside has been widely used for skin injuries owing to its significant therapeutic effect on promoting cell proliferation and collagen production, inhibiting inflammation, and preventing scar overgrowth, summarized as "5A" effects (antibacterial, antioxidant, anti-inflammatory, antihyperglycemic, and anti-ulcer) depicted in Fig. 1c. Figure 1d describes the schematical iontronic sensing mechanism of the SSWD. The sensing unit consists of an interdigital electrode and an ionically active gel layer with a built-in elastic and micro-hemispherical array. The ionic liquid [EMIM] [OTF] is introduced to form an electrical double layer (EDL) capacitance. The mechanical response is primarily based on the structural deformation of the hemispherical micro-structures, which exhibit ionic conductivity in contact with the planar electrode surfaces. A positive correlation exists between the interface capacitance and the contact area, resulting in an area expansion of the elastomer-electrode contact and a corresponding elevation in the EDL capacitance.

2.2 Fabrication and characterization of Janus organic hydrogel

To achieve multifunctional properties during wound management, the Janus organic hydrogel exhibits distinctly different characteristics on its two sides: a non-adhesive upper layer and an adhesive lower layer, respectively. Figure 2a presents the chemical components and cross-linking networks of the Janus organic hydrogel. The primary structure of this Janus organic hydrogel is based on acrylamide polymerization, using MBAA as the chemical crosslinker and introducing PEO and nanoclays to strengthen the network via hydrogen bonding. Specifically, PEO possesses good electronegativity to provide extensive hydrogen bonds within the gel via chain entanglement. Nanoclay (Laponite XLG) is a disk-shaped particle with a negative surface and positive edge, endowing strong hydrogen bonding formed between polymer chains and clay nanosheets [32].

Two strategies have been employed to build the upper and lower layers with different characteristics. Firstly, by changing the proportion of MBAA and the content of PEO and nanoclays, cross-linking density can be modulated. The upper layer has enhanced interactions of both the chemical and physical bonds, providing comprehensive mechanical properties. Secondly, introducing a dopamine structure rich in o-diphenol towards the lower layer brings high adhesion to different substrates, thus ensuring the stability and effectiveness of the wound dressing. Figure 2b further illustrates the adhesion characteristic of the lower layer towards various substrates in detail, including plastic, glass, metal, rubber, and skin. The extensive hydroxyl, amino, and amide groups in the gel can mainly form hydrogen bonds with different surfaces (for metal surfaces, electrostatic interaction can be formed). The interface between the two layers can be observed as shown in Fig. 2c, presenting a clear boundary and tight bonding observed under the optical microscope. The morphologies are also characterized using SEM. Notably, the upper layer presents a dense structure with smaller pores, indicating higher cross-linking density. In comparison, the lower layer shows uniform and larger pores due to lower cross-linking density. Figure 2d presents the adhesion behaviors of the two layers by peeling off the gel separately from the skin. The non-adhesive upper layer can be easily peeled off due to its dense cross-linking and lack of hydroxyl groups, which makes it difficult to provide non-covalent bonding between the skin but beneficial for subsequent sensing properties. However, the adhesive lower layer forms a tight bond towards the skin, aided by dopamine incorporation and a looser cross-linking structure, making it suitable for wound dressing to facilitate healing and release anti-inflammatory drugs.

For the upper layer, good flexibility and large deformability are essential not only for the overall structural stability of the intelligent wound dressing, but also for subsequent sensing functions, such as rapid perception of weak pressure signals. The mechanical properties of different gel components have been tested to optimize the upper layer, as shown in Fig. 2e. The gel network formed by covalent cross-linking using acrylamides as the monomer exhibits poor mechanical property, which can be improved by adding polymers or inorganic fillers to construct non-covalent bonding. The compression curves for the original AM gel, gel with added clay, gel with added PEO, and gel with both clay and PEO added simultaneously are plotted. Results demonstrate increasing compression strength in



sequence, from 0.92 Mpa, 1.26 Mpa, 2.98 Mpa, to 3.74 Mpa. Correspondingly, the elastic modulus of the gel decreases from 957 kPa, 939 kPa, 590 kPa, to 455 kPa (Fig. S1). PEO with a long chain structure can provide extensive hydrogen bonding sites, and the dissociation of polymer-nanoclay interactions can consume a lot of energy and delay the destruction of the hydrogel network [33]. Thus, the addition of both PEO and clay can significantly improve the mechanical properties of the upper gel with a high compression deformation degree of 95%, serving as the ideal material for pressure sensing.

◂**Fig. 3** Characterization of biocompatibility, antibacterial properties, hemostasis, and wound healing functions of the gels. **a** Fluorescence microscopy images of live/dead staining (green: live, red: dead) on NIH 3T3 cells cultured with control and gel (scale bars, 200 μm). **b** Cell viability calculated from the live/dead assay. **c**, **d** Images and optical density measurements of *S. aureus* and *Candida albicans* on Luria-Bertani medium with or without functional gel after 24 h. **e** Hemostasis process image for gauze, blank, and hydrogel. **f** Optical photographs of the hemostatic performance of the mouse liver bleeding model. **g** Optical photos of mice with subcutaneous gel implantation and those with only surgical suturing. **h** H&E staining of mouse liver and spleen tissues on day 7 (scale bars, 100 μm). **i** Schematic diagram of the skin wound healing model in mice. **j** Digital photographs of the wounds at different time points after different treatments. **k** Visual traces of the wound healing process. **l** Quantitative analysis of the wound area over different time points. **m** H&E staining of wound healing regions on day 10

As the lower layer directly contacts the skin, it is essential to provide good adhesion and durability for stable interfacial interactions between the gel and the skin surface for further wound healing. The self-healing property and adhesion characterization towards different substrates of the lower layer are shown in Fig. 2f–h. By cutting the stained gel into two pieces and placing them in contact, the two pieces healed after 24 h and could withstand tensile deformation of nearly twice the original length, presenting excellent self-healing property. The self-healing mechanism relies on the synergistic effects of multiple components. Specifically, PEO provides abundant ether bonds and terminal hydroxyl groups to form extensive hydrogen bonding within the polymer network that can temporarily reconnect fractured interfaces. The o-diphenol groups in dopamine provide stronger hydrogen bond donors and acceptors to facilitate dynamic cross-linking formation. Additionally, dopamine can engage in reversible coordination reactions with metal ions dissolved from the nanoclay. The nanoclay with its large specific surface area can form strong interactions with PAM, PEO, and dopamine through physical adsorption. Lap-shear testing is performed using a mechanical testing machine to quantify the adhesive strength of the lower layer on various substrates according to Fig. 2g [34]. In Fig. 2h, the adhesive force is deemed as the peak of the lap-shear curve. A gradual peel-off process with a long stripping lag phase is observed in most displacement curves. The adhesive forces of the lower layer against PI, rubber, copper, glass, and PET are 2.40, 3.08, 1.93, 2.38, and 1.88 N, respectively, indicating good interface integration to facilitate highly conformal contact and improve the reliability and stability of the wound dressing. To verify the applicability of gel dressing in the scene close to human skin, the adhesive properties of the SSWD towards pig skin have been evaluated (Figs. S2 and S3). Results indicate clear and significant adhesion observed at the interface, confirming the effective bonding of the SSWD under both dry and wet conditions.

To illustrate the durability of the SSWD, we have supplemented the cyclic tensile loading-unloading test at 25% strain (Fig. S4). After more than 100 cycles, it was able to retain its original shape, demonstrating excellent elasticity. Long-term stability is essential for wound dressing to ensure sustained effectiveness during the wound healing process. For traditional hydrogels, water is inevitably lost by evaporation under ambient conditions, causing the hydrogels to dry and harden, which seriously weakens their flexibility and deformability. The organic hydrogel has been prepared using mixing solvents to prevent the loss of water and realize anti-freezing property. Glycerol is widely used as a well-known, nontoxic anti-freezing, and moisturizing agent. It can form strong hydrogen bonds with water molecules to disrupt the formation of crystal lattices of ice at low temperatures and prevent the evaporation of water at high temperatures [35]. Figure 2i shows the anti-freezing properties of both the upper and lower layers. After freezing for 24 h, the flexibility of the upper layer remains unchanged, withstanding large deformation and recovering. The lower layer maintains good interface adhesion when pressing and lifting up. Furthermore, the long-term stabilities of both layers are investigated by monitoring the weight loss and size of the gels. As seen from Fig. 2j, the weights of both gel layers remain virtually unchanged ($<3\%$) after placing them under the ambient environment during the entire test cycle for 4 weeks, implying no shrinkage or water loss. In addition, no noticeable change in their geometric dimensions has been observed. The swelling ratio tests (Fig. S5) verify the stability of mechanical properties of the SSWD.

2.3 Characterization of the gel's biocompatibility, antibacterial properties, hemostasis, and wound healing functions

Cytocompatibility is a prerequisite for the gel to be used as a wound dressing. MTT and live/dead experiments were utilized to evaluate the biocompatibility of the prepared gel to NIH 3T3 fibroblasts, which play a critical role in the wound healing process. Figure 3a shows the staining results of live/dead cells; large green fluorescent dots (live cells) with a negligible amount of red fluorescent dots (dead cells) were observed in all groups. Meanwhile, the quantitative cell survival rates showed that the cell viability in all groups reached more than 90% (Fig. 3b), which confirmed the outstanding biocompatibility of the gel.

Bacterial or fungal infection is another major concern in wound treatment, as it leads to severe inflammation and hinders tissue healing. Figure 3c and d and Fig. S6 demonstrate the in vitro antibacterial ability of functional gel against *S. aureus* (Gram-positive bacterium) and *Candida albicans* (fungus) using an oxford cup method. Compared to the control group, almost no colonies were formed after

12 h coculturing the functional gel with *S. aureus* until 24 h. The functional gel exhibited excellent antibacterial properties that significantly reduced *S. aureus* and *Candida albicans* cell viability. Importantly, the antibacterial activities of functional gel are effective against not only the bacterial strains but also the fungal strain. Considering practical clinical application, an antibacterial test experiment using functional hydrogel on *Pseudomonas aeruginosa* (a clinically relevant pathogen in hospitals) has been conducted. Results show that it has a very good antibacterial effect (Fig. S7).

Hemostasis is the first stage of wound healing, so the gel patch used for wound healing should have hemostatic properties. Coagulation time is the most direct method to evaluate the hemostatic ability of materials. We evaluated the gel's hemostatic performance by simulating in vitro clotting time, as shown in Fig. 3e. It can be seen from the comparative experimental results that after 10 min, the gauze only has a partial coagulation effect, while the gel can achieve complete coagulation. The reason may be that the surface of the gel contains numerous hydrophilic groups, which can absorb the liquid and achieve the clotting effect [6]. The gel was applied to bleeding mouse livers damaged by an 18-gauge needle puncture to evaluate its hemostatic efficacy. Optical photographs comparing untreated livers and gel-treated livers are shown. Figure 3f presents images of filter papers used at time intervals from 0 to 90 s after gel application. In the blank group, a significant amount of blood was observed on the filter paper throughout the period, indicating a failure to achieve hemostasis. In contrast, almost no blood was detected on the filter paper in the gel-treated group. The gel patch significantly reduced bleeding, demonstrating effective hemostatic performance.

To evaluate the in vivo biocompatibility, the gel was fabricated into a wound-dressing patch and tested in a mouse model. Following subcutaneous implantation, the mice were sacrificed after 7 days for analysis (Fig. 3g). Histological examination and hepatotoxicity assays were conducted, including H&E staining of liver and spleen tissues. The results showed no signs of tissue toxicity at the implantation site (Fig. 3h), and all blood parameters fell within normal ranges (Table S1), confirming the good biosafety of the gel. Moreover, the wound healing capacity of the gel was evaluated via a mice dorsal full-thickness skin defect model infected with *S. aureus* (Fig. 3i). As shown in Fig. 3j, in order to compare with the gel group, the wounds of the control group were treated with standard wet gauze. The progress of wound healing was systematically recorded by capturing digital images at 0, 3, 7, and 10 days, respectively, focusing particularly on the analysis of wound closure trajectories. Moreover, to observe the closure variation, a stacked placement of the wound area and the rate of wound healing area in different treatment groups at different times was quantitatively analyzed, as shown in Fig. 3k and l. Visually on day 7, compared to the gel group, the wound surface of the control group had significant swelling due to bacterial infection and the wound healing area ratio was −15%. On day 10 of treatment, the wound healing area of the control, blank gel, and functional gel group were 27%, 83%, and 94%, respectively. These results suggested that blank gel also plays a role in wound healing, as it can provide a moist environment for wound regeneration and prevent the re-invasion of external pollutants. Meanwhile, asiaticoside in the gel plays an important role in promoting wound healing, attributed to its excellent antibacterial ability.

To further evaluate the details of the wound healing process, hematoxylin and eosin (H&E) staining pathological examinations were performed for histological analysis. As shown in Fig. 3m, tissues in the wounds of the control, blank gel, and functional gel groups were stained with H&E on day 10. In both the control and blank gel groups, large numbers of inflammatory cells were observed, indicating that serious inflammation remained unchecked due to the absence of antibacterial activity in these treatments. However, only a small number of neutrophils appeared in the wound tissues of mice treated with the functional gel, which was ascribed to its excellent capability against bacterium and fungus. Notably, new blood vessels and regenerated epidermis were observed in both the blank gel and functional gel groups, demonstrating that wound healing was accelerated by gel treatment [36]. However, wounds treated with the functional gel had more regenerated collagen deposition than the other two groups, further confirming the superior wound healing effect of the functional gel [6].

2.4 The sensing performances of the SSWD

To fabricate an ionic gel with a hemispherical surface structure, start by creating a photoresist template featuring a hemispherical array through photolithography. Then, a hemispherical polydimethylsiloxane (PDMS) negative mold is obtained by transferring the pattern from the photoresist. Next, the ionic gel precursor is poured into the PDMS mold, and the ionic gel with a hemispherical structure is achieved through UV curing, as shown in Fig. 4a. The SEM image of the structured ionic gel surface is shown in Fig. 4b.

Ideally, the SSWD should possess a pressure sensing range tailored to accommodate the diverse monitoring needs across various wound types and stages, coupled with outstanding static and dynamic sensing characteristics throughout this range. To comprehensively assess and optimize the sensing capabilities of the SSWD, we set up the sensing unit with a 1×1 cm^2 sensing area for testing purposes. Key device parameters such as sensitivity and sensing range can be inferred from the capacitance-to-pressure curve. As illustrated in Fig. 4c, the SSWD exhibited remarkable capacitance response across an extensive pressure spectrum

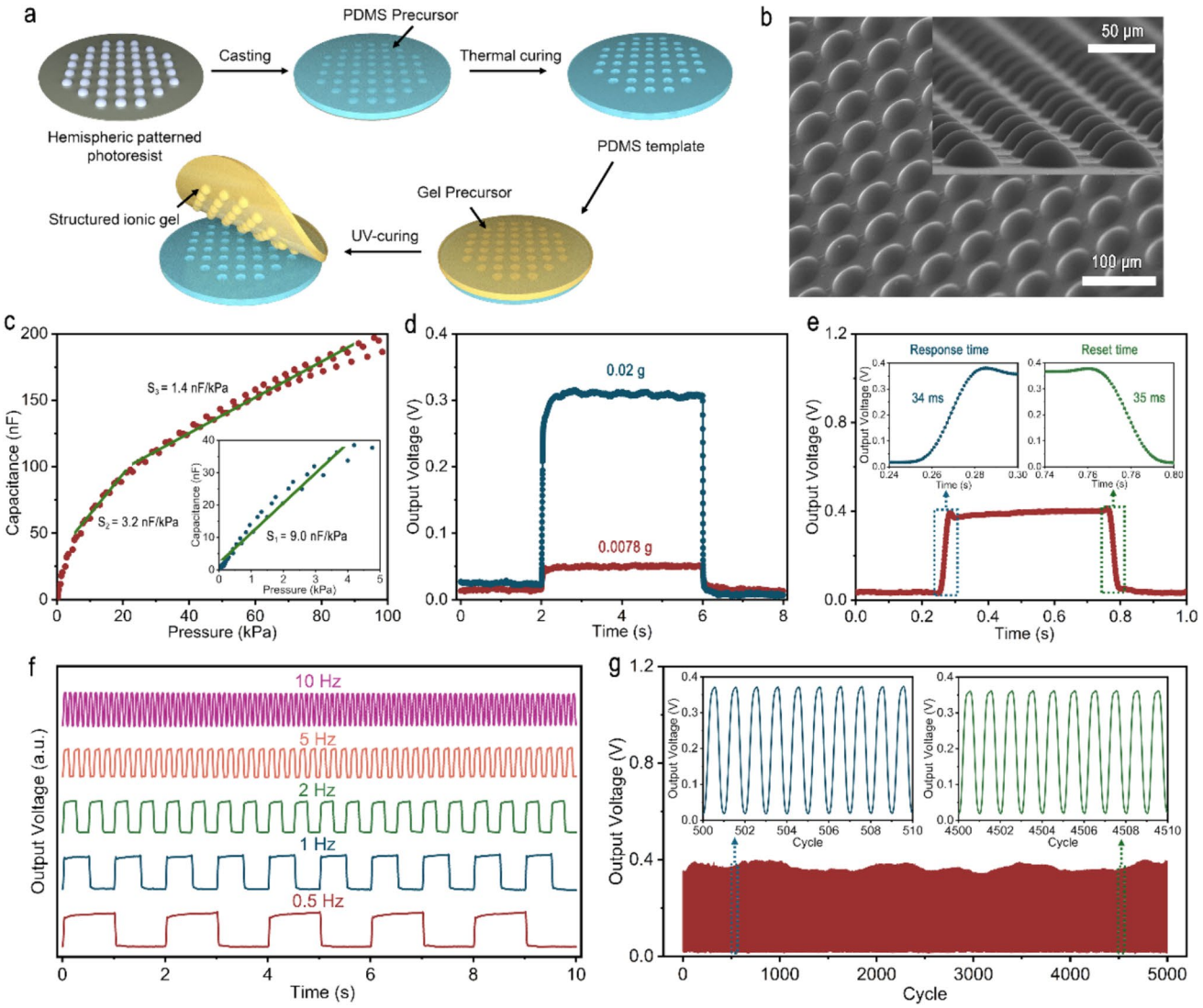


Fig. 4 Sensing performances of the SSWD. **a** Flow chart of structured ionic gel preparation. **b** SEM image of the structured ionic gel surface. **c** Capacitance-to-pressure curve for the sensing unit of the SSWD. **d** Output voltage curves recorded during the loading and unloading phases when subjected to ultralow pressures using two cotton balls of different weights. **e** Response and reset times. **f** Output voltage curves of the SSWD sensing unit under different dynamic stimulation ranging from 0.5 Hz to 10 Hz. **g** The output repeatability and stability of the SSWD sensing unit are sustained under cyclic mechanical loads at 10 Hz for 5000 cycles

of 0 to 100 kPa. Of particular interest, the inset in Fig. 4c highlights that within the low-pressure range of 0–5 kPa, the sensor achieved an average sensitivity of 9.0 nF/kPa. This sensitivity decreases as pressure increases: within the moderate pressure range of 5–20 kPa, the sensor's average sensitivity was 3.2 nF/kPa, and within the higher-pressure range of 20–100 kPa, it further reduced to an average of 1.4 nF/kPa. The wound healing process is inherently gradual, and its progress is seldom immediately apparent. To accurately track the nuanced progression of wound healing, the SSWD should possess exceptional pressure resolution capabilities, ensuring precise capture of even the most minute alterations in the healing process. We placed 0.02 g and 0.0075 g cotton balls on the sensor for approximately 4 s, then removed them and recorded the sensor's output voltage throughout the entire process. The experimental results, depicted in Fig. 4d, demonstrate successful ultralight object detection at the level of several tenths of a Pascal (approximately 0.78 Pa). The SSWD, tasked with monitoring external stimuli to prevent secondary wound damage during the healing process, utilizes a piezoelectric actuator driven by square wave signals of various frequencies to periodically apply mechanical loads of fluctuating frequencies to its sensing unit. As illustrated in Fig. 4f, the SSWD exhibits an outstanding dynamic response to external stimuli in the range of 0.5 to 10 Hz, characterized by minimal delay and hysteresis.

A response time of 34 ms and a reset time of 35 ms can be extracted from a single pressure cycle at a frequency of 1 Hz, as shown in Fig. 4e. Such rapid response and reset times ensure accurate monitoring of quick changes in external stimuli. Repeatability and stability assessments were performed using periodic loads at a frequency of 10 Hz. As depicted in Fig. 4g, the SSWD demonstrated exceptional stability and repeatability. This is evidenced by the initial output voltage with no pressure load and the peak output voltage under pressure, both of which remained nearly unchanged after 5000 pressure cycles.

2.5 Applications of the smart sensing wound dressing

2.5.1 Intelligent sensing wound dressing for infant wound touch warning

Infants, as a special group, require heightened attention in healthcare. Notably, they are highly vulnerable and unable to articulate their health complaints such as pain, discomfort, or sensations, or to manage these issues effectively [37]. Wound dressings protect wounds from infection and promote healing in cases of trauma. However, infants lack self-protection awareness and are prone to scratching the wound area or accidentally bumping it during the healing process, leading to secondary injuries and prolonging rehabilitation. Also, it is difficult for adults and guardians to maintain constant vigilance. Therefore, establishing one anti-touching wound dressing with alarm functions can realize monitoring of the wound status [20]. Sensors with high sensitivity can respond to slight pressure signals, triggering the device's alarms and drawing attention, thus avoiding potential risks caused by infant's unconscious touching of the wound. As shown in Fig. 5a, an infant model has been used to conduct the demonstration. The smart wound dressing is fixed onto the arm, where the adhesive side can achieve good adhesion to the skin, while the non-adhesive side faces outward with tactile sensing. The alarming device consists of a buzzer and an LED light and is fixed onto the chest of the infant. The circuit diagram of the entire device is shown in Fig. 5b, and the voltage of the external DC power supply is controlled at 6 V. The EDL capacitance of the sensing component varies and changes with the contact area between the functional gel and the electrode. In non-contact situations, the contact area is negligible and the circuit is disconnected. Upon touching the wound, the EDL capacitance increases significantly, accompanied by a current, thus simultaneously triggering the LED light and the buzzer alarm and indicating the risk of accidental touch. The video in Supporting Information (Supplementary Movie 1) demonstrates the smart wound dressing's alarm activation upon touching. This can achieve comprehensive medical healthcare management not only for infants but also for special populations with expression or cognitive impairments.

2.5.2 Flexible, high-resolution sensing array for wound management

The type of wound varies depending on its cause of injury, such as laceration, sharp injury, or abrasion, each presenting distinct wound appearances and morphologies. During rehabilitation, the morphology of the wound site changes due to processes like cell epithelialization and proliferation. For instance, obvious contraction occurs during the healing process of open injuries. Leveraging its high spatial resolution, a smart wound dressing with a pressure sensing array can comprehensively evaluate wound status via intuitive reproduction of the wound morphology. The pressure sensing array requires a high enough resolution to accurately reflect the morphologies of small wound sites. A high-density tactile array containing 32×32 sensing units has been implemented, resulting in a highly compact matrix structure with a spatial resolution of 0.44 mm center-to-center, equivalent to an array density of 522 points/cm^2, as illustrated in Fig. 5c. The positive and negative poles of each interdigital electrode unit are prepared as small circles with a diameter of 250 μm. All positive poles are connected into 32 columns, while the negative poles are connected into 32 rows from the back of the substrate using the metallized through-hole on each pole [38]. The high-sensitivity iontronic mechanism guarantees resolution, even at sub-millimeter scales. The ability to visually reproduce wound morphology of the SSWD has been validated by simulating different wound shapes. Figure 5d illustrates tactile recognition mappings of simulated wounds with different morphologies, including X-shaped, circular, elliptical, and laceration wounds. Notably, the wound dressing, with high spatial and pressure resolutions, distinctly recognizes and reproduces various morphologies, which can be beneficial for identification of wound types and monitoring morphology changes during the wound healing process.

In addition, wound swelling may occur during healing, especially for postoperative wounds, which are usually caused by wound fluid accumulation–induced tissue edema, infection, inflammatory stimulation, or fat liquefaction. It is essential to conduct timely targeted wound treatments based on swelling severity. Traditional wound dressings may mask the swelling behavior, leading to delayed detection and increased treatment costs. Different from a single sensing unit that monitors only pressure values, the sensing array can visually record the dynamic recovery status of the entire wound bed region. We construct scenarios to simulate wounds under various swelling conditions and monitor their status. The SSWD, equipped with a pressure sensing array, can achieve real-time mechanical image feedback of wound swelling. The light, flexible, and conformal wound dressing

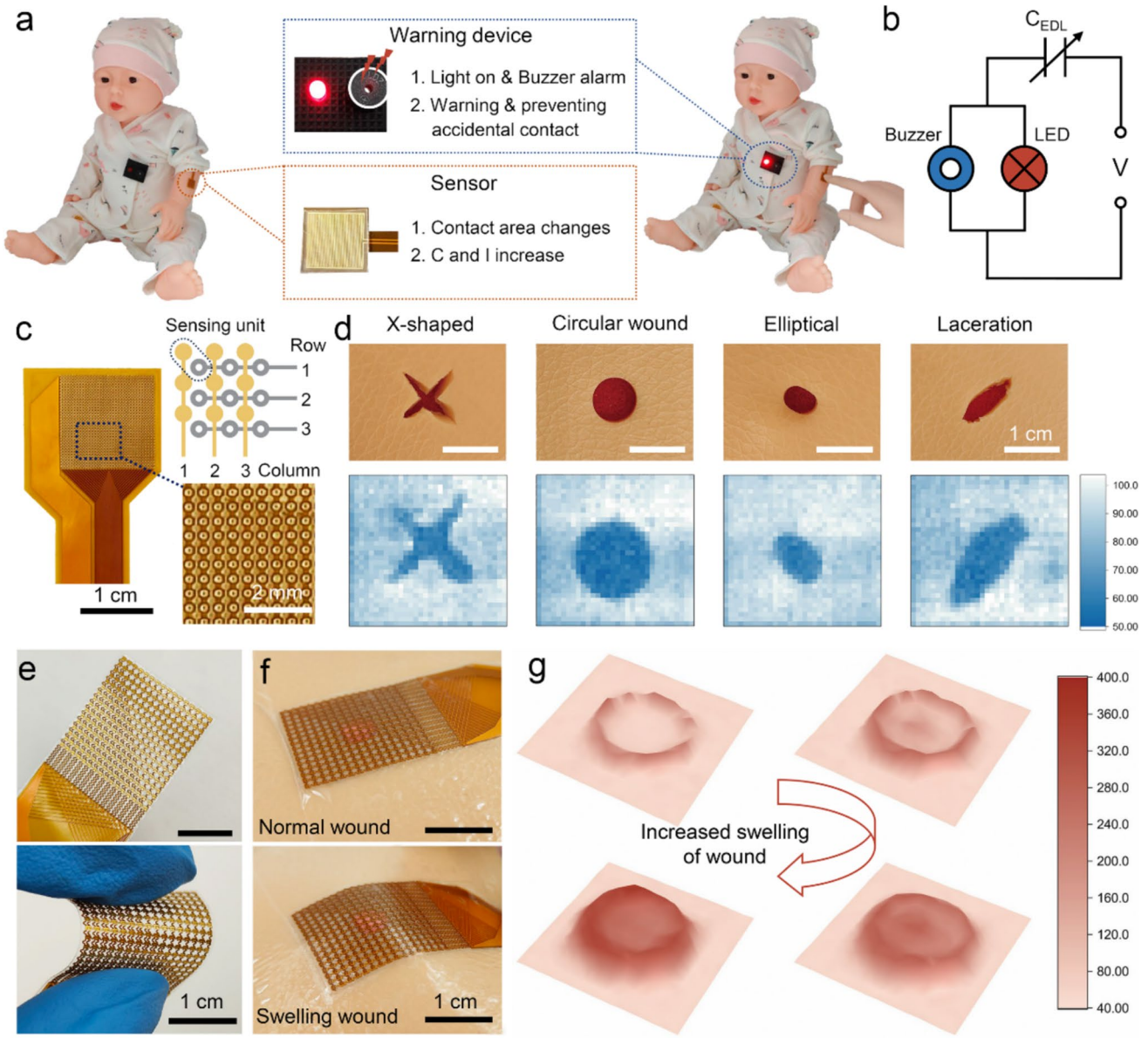


Fig. 5 Applications of the SSWD. (a) Demonstration of an infant wound touch warning system. (b) Circuit diagram of the entire device. (c) Photograph and microscopic image of the high-density sensing arrays containing 32×32 units. (d) Tactile mappings of wounds with different morphologies. (e) Photographs of the flexible electrode array under deformation. (f) Conformality of the flexible electrode array on the skin. (g) Three-dimensional pressure mappings with increasing degrees of wound swelling

can accurately perceive pressure signals, reduce motion artifacts, and avoid patient discomfort. To achieve good conformality to the skin surface, we have designed a flexible and stretchable tactile array containing 16×16 sensing units within an area of 2×2 cm^2. The electrode array is based on a deformable serpentine interconnect design [39]. After removing PI regions without interconnections via laser cutting and through thermal transferring to flexible substrates such as TPU and EVA, the electrode array, equipped with an island-bridge structure via serpentine interconnects, has been constructed, presenting good flexibility to withstand 180° bending, as shown in Fig. 5e and Fig. S8. The soft substrate of the electrode array serves as the encapsulating material, ensuring stable fitting and high conformality, as shown in Fig. 5f. Integrated with the functional gel, the electrode array has been placed onto the simulated wound bed as an SSWD. Figure 5g demonstrates three-dimensional pressure mappings with increasing wound swelling degrees. The mapping area and amplitude respectively reflect the size of the wound bed and the pressure caused by skin deformation. As swelling increases, the pressure loaded on the skin is enhanced; correspondingly, the pressure mappings

display size expansion and color darkening, thus providing real-time feedback on the wound status. In addition, this paper compares some existing intelligent wound dressings (Table S2), and we innovatively propose combining wound dressings with pressure sensor arrays to form smart sensing wound dressings, providing a new scheme for promoting wound healing.

3 Conclusion

The healing of traumatic and surgical wounds is a major challenge that puts tremendous strain on healthcare systems and patients. Among the most common complications of these wounds are bleeding, infection, impaired healing, and hypertrophic scarring. In summary, we have devised a multifunctional Janus organic hydrogel that exhibits biocompatibility, self-healing capabilities, and anti-freezing and moisturizing properties, as well as adjustable adhesion, serving as smart sensing wound dressings (SSWD) to promote wound healing and monitor wound status. The inherently adhesive Janus organic hydrogel (lower layer) directly covers the wound surface, acting as a barrier to prevent bacterial invasion. It synergizes with asiaticoside to enhance hemostasis, antibacterial, and anti-inflammatory effects. In the meanwhile, it can provide a favorable moist environment for wound regeneration and epithelialization, significantly improving the efficiency of wound healing.

Furthermore, the non-viscous Janus organic hydrogel (upper layer) is endowed with an iontronic pressure sensing function, characterized by high sensitivity (the maximum was about 9.0 nF/kPa), low detection limits (approximately 0.78 Pa), fast response time (34 ms), and high stability ($\geq$ 5000 cycles). This sensing system enables real-time, in situ monitoring of physical changes surrounding the wound, providing early indications of swelling due to infection or collisions. Combined with a high-density array of electrodes, it achieves accurate pressure detection with a spatial resolution of 0.44 mm center-to-center (array density of 522 points/cm^2), facilitating real-time or remote, in situ visual monitoring of wounds. This empowers medical professionals to intervene promptly and effectively. Therefore, the integration of wound dressings with pressure sensing, using organic hydrogels to create smart sensing wound dressings as presented in this study, marks a significant contribution to transformative healthcare solutions. It exemplifies a strategic approach aimed at optimizing the recovery of patients with skin trauma, representing a substantial advancement in wound care management.

4 Experimental section

4.1 Fabrication of Janus organic hydrogel

The Janus organic hydrogel was fabricated with a two-step photo curing of the adhesive layer and non-adhesive layer successively, using the mixed solvent (glycerol and water) with the ratio of 1:1. First, 3.0 g acrylamide (AM, 99%, Aladdin reagent company), 0.01 g crosslinker N, N′-methylenebis(acrylamide) (MBAA, 99%, Aladdin reagent company), and 0.6 g polyethylene oxide (PEO, 97%, MW ~ 1,000,000, Aladdin reagent company) were dissolved in 20 mL glycerol/water mixed solvent, followed by adding 0.2 g asiaticoside (99%, Chengdu Biopurify Co., LTD), 0.1 g clay (Laponite XLG, BYK Additives Inc.), 0.4 g dopamine hydrochloride (DA, 99%, Aladdin reagent company), and 0.6 g initiator 2-Hydroxy-2-methylpropiophenone (HMPP 1173, 99%, Aladdin reagent company). The mixed solution was stirred for 2 h to form the gel precursor I. Afterwards, nitrogen (99.99%, Hongzhou Industrial Gas Co., LTD) was pumped into the precursor for 20 min to exclude the oxygen. Finally, the precursor solution was injected into the lab-made curing cell consisting of two release films with a tunable gap for expected gel thickness, followed by UV (365 nm, 36 W) exposure in a UV curing chamber for 2 min to form the adhesive layer.

The non-adhesive layer with hemispheric micro-structure was cured on the basis of the adhesive layer to achieve tight integration. Similarly, 6.0 g AM, 0.12 g MBAA, and 0.2 g PEO were dissolved in 20 mL glycerol/water mixed solvent, followed by adding 0.2 g 1-ethyl-3-methylimidazolium trifluoromethanesulfonate ([EMIM][OTF], 99%), 0.2 g clay, and 0.6 g initiator 1173 to form the gel precursor II. The micro-structure of the non-adhesive layer was constructed via templating. The original photoresist template with hemispheric structure was processed according to our previous work [38]. PDMS precursors (Sygard 184, Dow Company) were cast and cured at 80 °C for 2 h, thus transferring the micro-structures of the photoresist template onto the surface of a PDMS mold. After pumping the nitrogen, the precursor was poured onto the adhesive layer and covered with the PDMS mold to expose UV light for 2 min to form the non-adhesive layer. After peeling from the mold, the Janus organic hydrogel was obtained with the adhesive side and ionic non-adhesive structured side.

4.2 Mechanical tests

A compressive test of the non-adhesive gel was performed by a motorized force tester (ESM 303, Mark-10) with a 1 kN load cell at room temperature. The gel samples were

prepared into cylinders with a diameter of 13 mm and a height of 4 mm. The testing velocity was 0.5 mm min^{-1}. Three parallel specimens were repeated. The cyclic tensile loading-unloading test was conducted with the sample size of $20 \times 10 \times 2$ mm. The self-healing behaviors of the adhesive gel were investigated. First, two adhesive gels were dyed with different colors and cut in half separately. Subsequently, two halves of gels were put together at room temperature and left for 48 h to ensure total healing. The self-healing gel was stretched and compared the length before and after stretching. The anti-freezing properties of both the adhesive and non-adhesive gels were performed after −20 °C freezing for 48 h. The samples were cut into squares with an area of 13×13 mm^2.

4.3 Adhesion measurement

The adhesion strengths of gels on various material surfaces (PET, PI, glass, copper, and NBR) were executed by lap-shear tests using a motorized force tester (ESM 303, Mark-10) equipped with a 50 N load cell and at a constant speed of 50 mm min^{-1}. The gel was sandwiched between two material surfaces with an adhesion area of 10×10 mm^2 and left for 12 h before conducting the test. Considering actual clinical applications, the adhesion strengths of gels on pig skin were executed.

4.4 Long-term water retention test

Long-term water retention was assessed by recording the weight change of the gels weekly. The relative humidity of the environment was controlled at 45%. The weight retention ratio was calculated by the following equation:

$$WRt = \frac{W_t}{W_0} * 100\%$$

W_t and W_0 represent the recording weight and the initial weight of gels, respectively. Three parallel specimens were tested.

4.5 Characterization and measurement setup of the sensing properties

The morphologies of the ionic non-adhesive structured layer were characterized using SEM (Sigma 300, Zeiss). All test samples experienced lyophilization at −60 °C for over 24 h after freezing for over 12 h. The capacitance-to-contact pressure curves were tested by recording the capacitance readouts of the smart wound dressing under increased contact pressure applied by the motorized force tester. The scanning frequency and voltage are set to be 1 kHz and 1 V respectively. The response/reset time and the repeatability were measured by applying a periodic pressure of 1 and 10 Hz, respectively, by a piezoelectric actuator (PB4NB2S, Thorlabs Inc.). A signal generator (AFG1022, Tektronix) is used to apply a periodical square wave of ± 5 V to the electromagnetic relay. The readouts were amplified through operating amplifier circuitry and recorded by a data acquisition card with an extremely high sampling rate of 1 M/s (DAQ, NI USB-6361, NI instruments). Mechanical responses of the smart wound dressing under varied periodic stimuli of 0.5 Hz, 1 Hz, 2 Hz, 5 Hz, and 10 Hz. The readout circuitry for the single point sensor of the smart wound dressing is shown in Fig. S9. The readout circuitry for the sensing array was mainly composed of a column selection unit (MUX), data acquisition unit (ADC), digital-to-analog converter (DAC), and control unit (FPGA) (Fig. S10).

4.6 In vitro cell compatibility tests

MTT assay was conducted to evaluate the in vitro cytocompatibility and potential cytotoxic effects of the synthesized gels on NIH3T3 cells by assessing their metabolic activity. NIH3T3 cell suspension was diluted with serum cell medium to a cell density of 10^4 cells mL^{-1}, seeded in 96-well plates, and incubated at 37 °C for 24 h in 5% CO_2 atmosphere. The gel was extracted using complete culture medium at a concentration of 0.2 g/mL to obtain a 100% concentration original leachate. For the control group, the complete cell medium was used. For the experiment group, the 100% extract was diluted into a series of concentrations (e.g., 100%, 50%, 20%) for cell culture. After cultivating for 24 h, 72 h, and 120 h, discard the supernatant, and rinse with PBS. Then, 200 μL MTT (HY-15924, MCE) was added at a concentration of 0.5 mg/mL to each well and cultivated for 4 h. After adding DMSO (200 μL) to each well and shaking for 10 min, absorbance (A) of each sample at 570 nm was detected using an enzyme-linked immunosorbent assay (ELISA) reader (EPOCH2, Biotech). The cell viability was calculated by the following equation:

$$CA(\%) = \frac{A_{sample}}{A_{control}} * 100\%$$

4.7 Evaluation of antibacterial activity

C. albicans and *S. aureus* were incubated separately in YPD liquid medium and LB liquid medium at a speed of 190 rpm for 12 h with OD600 at 0.6. Gels were disinfected under UV light for 2 h, and then put into the above diluted liquid medium for further culture. The control group consisted of bacterial suspension without the functionalized gel dressing. OD600 absorbance values were detected after cultivating for 12 h, 18 h, and 24 h. The collected bacterial suspension

was inoculated onto nutrient agar plates and incubated for 24 h. Finally, the antibacterial activity was visually evaluated through the number of bacterial colonies.

4.8 In vitro coagulation and hemostatic property

In vitro, clotting time was recorded by selecting the blank group, gauze group, and gel group. Ten milligrams of each sample was incubated at 37 ℃ for 10 min. One hundred microliters CWB of adult female rabbits was incubated at 37 ℃ for 10 min. Subsequently, incubated blood was introduced into the sample tube, followed by adding 10 μL $CaCl_2$ solution (0.17 M). Monitoring the coagulation process at 37 °C, rotating the sample tube every 10 s until blood flow significantly stops, and then recording the clotting time. Each sample was tested at least three times. The hemostatic capability of the hydrogel was evaluated using a mouse liver hemorrhage model. An 18-gauge needle was inserted at approximately 30° relative to a soft cardboard platform to create a puncture wound. Quantitative filter paper was placed beneath the incision to absorb blood. Immediately after injury, the hydrogel was applied to the bleeding site. Photographs were taken at 0 to 90 s post-injury to document bleeding. Cumulative blood loss was calculated based on the weight change of the blood-stained filter papers.

4.9 In vivo animal experiment for wound healing monitoring

Male BALB/c mice of 6-week-old (Shanghai SLAC Laboratory Animal Co., Ltd) were equivalently and randomly divided into 3 groups: a blank group (no incision), a control group (underwent surgery without patch implantation), and a gel group (subcutaneously implanted with the hydrogel patch). All mice were euthanized 7 days after surgery. Blood samples were collected for complete blood count (CBC) analysis. Liver and spleen tissues were harvested for H&E staining to evaluate the potential toxicity of the patch. Additionally, a mouse model of full-thickness skin defect has been established to conduct wound healing experiment. The backs of mice were shaved, and pieces of full-thickness skin with 4 mm diameter on the back were excited, then opened the entire skin layer and penetrated deep into the fascia layer to create a skin wound model. *S. aureus* was added to the round wound bed after sufficient hemostasis with a concentration at 7.5×10^6 CFU/mL. After infection for 2 h, dressing treatment was given to the localized infected lesions. For the control group, a gauze patch was applied to the wound bed. For the blank gel group, a gel patch consisting of gel components without asiaticoside adhered to the wound. For the functional gel group, asiaticoside was introduced to the gel component. The healing process of the wound was closely monitored and documented with photographs on the postoperative days of 0, 3, 7, and 10, accompanied by an analysis of the wound size and healing area. Tissue samples were collected from the wound bed area at 7 and 10 days. All rats were sacrificed via spinal dislocation method. The whole animal experiments were reviewed and approved by the Human Participants Ethics Committee of Shanghai Normal University; the approval number is 2,024,106.

4.10 H&E staining for histological analysis

H&E staining was conducted on cross-sectioned tissues from the wound bed. The related tissues of the control group, blank gel group, and functional gel group were harvested and placed in the tissue fixative (G1101, Service bio) above 24 h, then treated with dehydration and wax immersion, embedding the tissue in paraffin (JB-P5) and sliced on a paraffin slicer (RM2016, Leica) with a thickness of 4 μm. The slides were sealed with paraffin and stored at room temperature. To conduct the H&E staining experiment, first put the slices into an environmentally friendly dewaxing solution (G1128, Service bio) to remove the paraffin and then rehydrated using ethanol and water. Afterwards, the slides were treated with pre-treatment solution for 1 min, and then performed hematoxylin staining for 3–5 min, differentiated, and blued. Then, the slides were dehydrated and stained with eosin for 15 s. Finally, the slides were dehydrated again through a series of graded alcohol solutions and cleared in xylene. After being sealed with neutral resin adhesive, the coloring situation was observed via an optical microscope (Nikon Eclipse E100).

Supplementary Information The online version contains supplementary material available at https://doi.org/10.1007/s42114-025-01510-y.

Acknowledgements The authors are grateful for the financial support from the Guangdong Basic and Applied Basic Research Foundation (2023B1515120010, 2022A1515011240, and 2025A1515012917), the National Key Research and Development Program Grant (2023YFF0721500), the National Natural Science Foundation of China (62101541 and 62101542), the Guangdong Program (2021TQ06Y105), the Natural Science Foundation of Shenzhen (JCYJ20220818101207017), the Science and Technology Planning Project of Shenzhen Science and Technology Innovation Commission (KCXFZ20230731100901004), the Innovation &Entrepreneurship leader program of Suzhou (ZXL2023153), the Zhejiang Provincial Natural Science Foundation of China (LQN25F010013), and Hangzhou Normal University Scientific Research Start-up Foundation (4305C50223204084).

Author contribution Y.C.1, S.L.2 and S.L.3 contributed equally to this work. J.L.3, H.Y.1 and H.S.1 contributed as the corresponding authors. Y.C.1, S.L.2, and H.S.1 conceived and designed the research. Y.C.1, S.L.2, and H.S.1 participated in hydrogel preparation, device fabrication, characterization and demonstration of SSWD. Z.Y.4, Y.C.5, Y.Z.6, B.S.1, and T.P.1 supported data collection and processing. J.L.3, S.L.3, and S.W.7 supervised the animal experiments and analyzed the data. Y.C.1, S.L.2, and H.S.1 wrote the manuscript. Y.H.1, and H.S.1 revised

the manuscript and supervised the research. All authors contributed to the discussion and analysis of the results.

Funding This research was supported by the financial support from the Guangdong Basic and Applied Basic Research Foundation (2023B1515120010, 2022A1515011240, and 2025A1515012917), the National Key Research and Development Program Grant (2023YFF0721500), the National Natural Science Foundation of China (62101541 and 62101542), the Guangdong Program (2021TQ06Y105), the Natural Science Foundation of Shenzhen (JCYJ20220818101207017), the Science and Technology Planning Project of Shenzhen Science and Technology Innovation Commission (KCXFZ20230731100901004), the Innovation & Entrepreneurship leader program of Suzhou (ZXL2023153), the Zhejiang Provincial Natural Science Foundation of China (LQN25F010013), and Hangzhou Normal University Scientific Research Start-up Foundation (4305C50223204084).

Data availability No datasets were generated or analysed during the current study.

Declarations

Conflict of interest The authors declare no competing interests.

Open Access This article is licensed under a Creative Commons Attribution 4.0 International License, which permits use, sharing, adaptation, distribution and reproduction in any medium or format, as long as you give appropriate credit to the original author(s) and the source, provide a link to the Creative Commons licence, and indicate if changes were made. The images or other third party material in this article are included in the article's Creative Commons licence, unless indicated otherwise in a credit line to the material. If material is not included in the article's Creative Commons licence and your intended use is not permitted by statutory regulation or exceeds the permitted use, you will need to obtain permission directly from the copyright holder. To view a copy of this licence, visit http://creativecommons.org/licenses/by/4.0/.

References

1. Peña OA, Martin P (2024) Cellular and molecular mechanisms of skin wound healing. Nat Rev Mol Cell Biol 25(8):599–616
2. Sun BK, Siprashvili Z, Khavari PA (2014) Advances in skin grafting and treatment of cutaneous wounds. Science 346(6212):941–945
3. Guo B, Dong R, Liang Y, Li M (2021) Haemostatic materials for wound healing applications. Nat Rev Chem 5(11):773–791
4. Wang C, Shirzaei Sani E, Shih C-D, Lim CT, Wang J, Armstrong DG, Gao W (2024) Wound management materials and technologies from bench to bedside and beyond. Nat Rev Mater 9(8):550–566
5. Liang Y, He J, Guo B (2021) Functional hydrogels as wound dressing to enhance wound healing. ACS Nano 15(8):12687–12722
6. Sun L, Zhou J, Lai J, Zheng X, Wang H, Lu B, Huang R, Zhang L-M (2024) Novel natural polymer-based hydrogel patches with Janus asymmetric-adhesion for emergency hemostasis and wound healing. Adv Funct Mater 34(36):2401030
7. Li C, Wang J-T, Liu K, Ding H, Li Q-F, Liang G, Jin L, He D (2024) Antibacterial and anti-inflammatory synergistic effects of double-layer hydrogel promoting bacterial wound healing. Chem Eng J 493:152513
8. Ren H, Zhang Z, Cheng X, Zou Z, Chen X, He C (2023) Injectable, self-healing hydrogel adhesives with firm tissue adhesion and on-demand biodegradation for sutureless wound closure. Sci Adv 9(33):eadh4327
9. Li Y, Wang Y, Ding Y, Fan X, Ye L, Pan Q, Zhang B, Li P, Luo K, Hu B, He B, Pu Y (2024) A double network composite hydrogel with self-regulating Cu2+/luteolin release and mechanical modulation for enhanced wound healing. ACS Nano 18(26):17251–17266
10. Dong R, Guo B (2021) Smart wound dressings for wound healing. Nano Today 41:101290
11. Zhao C, Park J, Root SE, Bao Z (2024) Skin-inspired soft bioelectronic materials, devices and systems. Nat Rev Bioeng 2(8):671–690
12. Han M, Chen L, Aras K, Liang C, Chen X, Zhao H, Li K, Faye NR, Sun B, Kim J-H, Bai W, Yang Q, Ma Y, Lu W, Song E, Baek JM, Lee Y, Liu C, Model JB, Yang G, Ghaffari R, Huang Y, Efimov IR, Rogers JA (2020) Catheter-integrated soft multilayer electronic arrays for multiplexed sensing and actuation during cardiac surgery. Nat Biomed Eng 4(10):997–1009
13. Xu G, Lu Y, Cheng C, Li X, Xu J, Liu Z, Liu J, Liu G, Shi Z, Chen Z, Zhang F, Jia Y, Xu D, Yuan W, Cui Z, Low SS, Liu Q (2021) Battery-free and wireless smart wound dressing for wound infection monitoring and electrically controlled on-demand drug delivery. Adv Funct Mater 31(26):2100852
14. Lu S-H, Samandari M, Li C, Li H, Song D, Zhang Y, Tamayol A, Wang X (2022) Multimodal sensing and therapeutic systems for wound healing and management: a review. Sensors and Actuators Reports 4:100075
15. Qiao Y, Luo J, Cui T, Liu H, Tang H, Zeng Y, Liu C, Li Y, Jian J, Wu J, Tian H, Yang Y, Ren T-L, Zhou J (2023) Soft electronics for health monitoring assisted by machine learning. Nano-Micro Lett 15(1):66
16. Kang K, Ye S, Jeong C, Jeong J, Ye Y-s, Jeong J-Y, Kim Y-J, Lim S, Kim TH, Kim KY, Kim JU, Kim GI, Chun DH, Kim K, Park J, Hong J-H, Park B, Kim K, Jung S, Baek K, Cho D, Yoo J, Lee K, Cheng H, Min B-W, Kim HJ, Jeon H, Yi H, Kim T-i, Yu KJ, Jung Y (2024) Bionic artificial skin with a fully implantable wireless tactile sensory system for wound healing and restoring skin tactile function. Nat Commun 15(1):10
17. Lu Y, Yang G, Wang S, Zhang Y, Jian Y, He L, Yu T, Luo H, Kong D, Xianyu Y, Liang B, Liu T, Ouyang X, Yu J, Hu X, Yang H, Gu Z, Huang W, Xu K (2024) Stretchable graphene–hydrogel interfaces for wearable and implantable bioelectronics. Nat Electron 7(1):51–65
18. Mostafalu P, Tamayol A, Rahimi R, Ochoa M, Khalilpour A, Kiaee G, Yazdi IK, Bagherifard S, Dokmeci MR, Ziaie B, Sonkusale SR, Khademhosseini A (2018) Smart bandage for monitoring and treatment of chronic wounds. Small 14(33):1703509
19. Xiao J, Zhou Z, Zhong G, Xu T, Zhang X (2024) Self-sterilizing microneedle sensing patches for machine learning-enabled wound pH visual monitoring. Adv Funct Mater 34(22):2315067
20. Yan R, Sun Z, Du W, Liu N, Sun Q, Li P, Liang F, Zhu Y, Huang W, Yu H-D (2024) An electrostatic-induction-enabled anti-touching hydrogel dressing for chronic wound care. Adv Funct Mater 34(37):2402217
21. Deng WJ, Wang LF, Dong L, Huang QA (2018) LC wireless sensitive pressure sensors with microstructured PDMS dielectric layers for wound monitoring. IEEE Sens J 18(12):4886–4892
22. Wu Q, Qiao Y, Guo R, Naveed S, Hirtz T, Li X, Fu Y, Wei Y, Deng G, Yang Y, Wu X, Ren T-L (2020) Triode-mimicking graphene pressure sensor with positive resistance variation for physiology and motion monitoring. ACS Nano 14(8):10104–10114
23. Sun H, Pan N, Jin X, Deng K, Liu Z, Lin C-T, Pan T, Chang Y (2020) Active-powering pressure-sensing fabric devices. J Mater Chem A 8(1):358–368
24. He Y, Cheng Y, Yang C, Guo CF (2024) Creep-free polyelectrolyte elastomer for drift-free iontronic sensing. Nat Mater 23(8):1107–1114

25. Guo Y, Yin F, Li Y, Shen G, Lee J-C (2023) Incorporating wireless strategies to wearable devices enabled by a photocurable hydrogel for monitoring pressure information. Adv Mater 35(29):2300855
26. Tang W, Sun Q, Wang ZL (2023) Self-powered sensing in wearable electronics—a paradigm shift technology. Chem Rev 123(21):12105–12134
27. Wang B, Liu C, Xiao Y, Zhong J, Li W, Cheng Y, Hu B, Huang L, Zhou J (2017) Ultrasensitive cellular fluorocarbon piezoelectret pressure sensor for self-powered human physiological monitoring. Nano Energy 32:42–49
28. Fan W, He Q, Meng K, Tan X, Zhou Z, Zhang G, Yang J, Wang ZL (2020) Machine-knitted washable sensor array textile for precise epidermal physiological signal monitoring. Sci Adv 6(11):eaay2840
29. Song Y, Wang N, Wang Y, Zhang R, Olin H, Yang Y (2020) Direct current triboelectric nanogenerators. Adv Energy Mater 10(45):2002756
30. Zhu P, Du H, Hou X, Lu P, Wang L, Huang J, Bai N, Wu Z, Fang NX, Guo CF (2021) Skin-electrode iontronic interface for mechanosensing. Nat Commun 12(1):4731
31. Chang Y, Wang L, Li R, Zhang Z, Wang Q, Yang J, Guo CF, Pan T (2021) First decade of interfacial iontronic sensing: from droplet sensors to artificial skins. Adv Mater 33(7):2003464
32. Zhang J, Shen S, Lin R, Huang J, Pu C, Chen P, Duan Q, You X, Xu C, Yan B, Gao X, Shen Z, Cai L, Qiu X, Hou H (2023) Highly stretchable and biocompatible wrinkled nanoclay-composite hydrogel with enhanced sensing capability for precise detection of myocardial infarction. Adv Mater 35(9):2209497
33. Zhang M, Yu J, Shen K, Wang R, Du J, Zhao X, Yang Y, Xu K, Zhang Q, Zhang Y, Cheng Y (2021) Highly stretchable nanocomposite hydrogels with outstanding antifatigue fracture based on robust noncovalent interactions for wound healing. Chem Mater 33(16):6453–6463
34. Hu R, Yang X, Cui W, Leng L, Zhao X, Ji G, Zhao J, Zhu Q, Zheng J (2023) An ultrahighly stretchable and recyclable starch-based gel with multiple functions. Adv Mater 35(42):2303632
35. Han L, Liu K, Wang M, Wang K, Fang L, Chen H, Zhou J, Lu X (2018) Mussel-inspired adhesive and conductive hydrogel with long-lasting moisture and extreme temperature tolerance. Adv Funct Mater 28(3):1704195
36. Ming Z, Han L, Bao M, Zhu H, Qiang S, Xue S, Liu W (2021) Living bacterial hydrogels for accelerated infected wound healing. Adv Sci 8(24):2102545
37. Yuan M, Long Y, Liu T, Liu J, Qiu S, Lin T, Xu F, Fang Y (2024) Soft electronics for advanced infant monitoring. Mater Today 75:166–186
38. Cheng Y, Guo C, Li S, Deng K, Tang J, Luo Q, Zhang S, Chang Y, Pan T (2022) Aquatic skin enabled by multi-modality iontronic sensing. Adv Funct Mater 32(48):2205947
39. Kim D-H, Song J, Choi WM, Kim H-S, Kim R-H, Liu Z, Huang YY, Hwang K-C, Zhang Y-w, Rogers JA (2008) Materials and noncoplanar mesh designs for integrated circuits with linear elastic responses to extreme mechanical deformations. Proc Natl Acad Sci USA 105(48):18675–18680

Publisher's Note Springer Nature remains neutral with regard to jurisdictional claims in published maps and institutional affiliations.